

ESD-TR-68-356

ESD-TR-68-356

ESD RECORD COPY

RETURN TO
SCIENTIFIC & TECHNICAL INFORMATION DIVISION
(ESTI), BUILDING 1211

ESD ACCESSION LIST

ESTI Call No. 65066

Copy No. 1 of 1 cys.

ESLE

121

Technical Report

459

LES-6 Triplexer

D. R. Bold
A. Sotiropoulos

2 December 1968

Prepared under Electronic Systems Division Contract AF 19(628)-5167 by

Lincoln Laboratory

MASSACHUSETTS INSTITUTE OF TECHNOLOGY

Lexington, Massachusetts



AD686418

MASSACHUSETTS INSTITUTE OF TECHNOLOGY
LINCOLN LABORATORY

LES-6 TRIPLEXER

D. R. BOLD

Group 63

A. SOTIROPOULOS

Group 61

TECHNICAL REPORT 459

2 DECEMBER 1968

This document has been approved for public release and sale;
its distribution is unlimited.

ABSTRACT

This report describes the design and development of the triplexer used in the UHF communications satellite LES-6. The triplexer is a four-port passive microwave structure which provides a common antenna port for simultaneous operation at the transmit, beacon, and receive frequencies, and consists of three interdigital band-pass filters connected by appropriate lengths of transmission line. A special feature of the transmit filter is its gas-filled hermetically sealed construction, and the details of the mechanical design of the pressure vessel are discussed.

Accepted for the Air Force
Franklin C. Hudson
Chief, Lincoln Laboratory Office

CONTENTS

Abstract	iii
I. Transmit (TX) and Beacon (BEC) Filters	1
II. Receive Filter	3
III. Triplexer	3
IV. Mechanical Design	6
V. Fabrication	8
Appendix	11

LES-6 TRIPLEXER

This report describes the design, development, and construction of the UHF bandpass filters used in Lincoln Experimental Satellite-6 (LES-6).^{*} Each filter is designed from the low-pass Chebyshev response and uses quarter-wave interdigital resonator elements.¹ Three filters were combined by appropriate lengths of transmission line into a four-port configuration which separates the transmit (TX), beacon (BEC), and receive (REC) frequencies. The triplexer arrangement is shown in Fig. 1. A telemetry (TLM) filter was also built; however, this unit is not a part of the triplexer. The TLM filter design is identical to the filter used in LES-5, and a discussion of it and a similar triplexer can be found in an earlier report.² This report will be concerned only with the TX, BEC, and REC filters and the combined triplexer assembly.

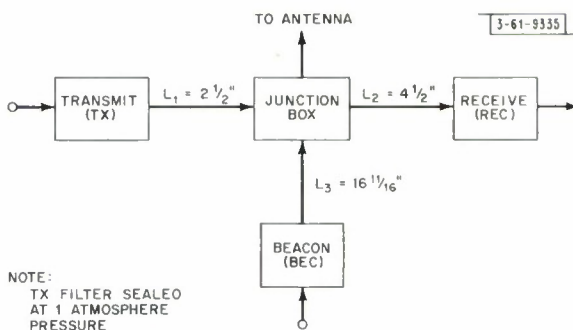


Fig. 1. LES-6 triplexer configuration.

Two important features characterize the LES-6 triplexer:

- (1) The TX and BEC frequency separation is only 5 MHz (≈ 2 percent of center frequency).
- (2) The TX filter is a gas-filled hermetically sealed unit.

The design calculations for the filters are essentially the same as those described in the aforementioned LES-5 triplexer report and will not be repeated here.

I. TRANSMIT (TX) AND BEACON (BEC) FILTERS

The LES-6 triplexer design requirements are shown in Fig. 2. The system specifications required approximately 40-dB rejection to the TLM frequency and 40-dB mutual rejection between the REC and BEC filters. The only way in which the 0.5-dB pass-band loss specification could be met was to double the unloaded Q from about the 1200 used in the REC and TLM filters to about 2400. This made it possible to achieve high out-of-band rejection combined with low pass-band loss at the TX and BEC frequencies with the penalty of a physically larger filter. The optimum design (lowest loss, maximum rejection) for both the BEC and TX filters proved to be a five-element Chebyshev interdigital design with a 0.01-dB ripple. The BEC and TX frequencies were then placed in the first null at the edge of their pass bands (see Fig. 3) to obtain maximum out-of-band rejection characteristics, and consequently each filter was tuned to favor those frequencies.

^{*} D. R. Bold was responsible for the mechanical design and testing, and Arthur Sotiropoulos was responsible for the electrical design and testing of this triplexer.

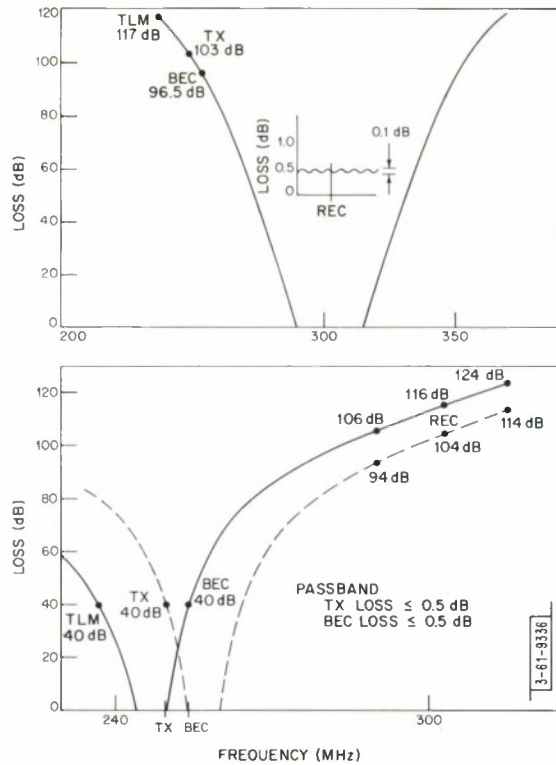


Fig.2. LES-6 triplexer design specifications.

The LES-5 transmit (TX) filter had experienced RF voltage breakdown in vacuum testing (approximately 10^{-6} mmHg pressure) due to the phenomenon of multipactoring.³ This problem was eliminated in LES-5 by completely filling the filter with a low-loss, low-dielectric constant foam. The same approach was initially planned and attempted on the LES-6 TX filter; however, because of geometry changes, higher voltages, and higher power levels than those of LES-5, the LES-6 foam-filled filter also experienced breakdown when operated in a vacuum at rated power. Many other dielectric materials were subsequently tried in various configurations: (1) polystyrene foam, (2) polyurethane foam, (3) quartz wool, (4) alumina, and (5) teflon. All these materials proved unsatisfactory for various reasons. The foam materials failed because of excessive heating, the quartz wool with its large surface area presented a severe out-gassing problem, and the alumina and teflon materials were much too heavy to warrant serious consideration as a final solution. It was then decided that the only obvious practical solution available was pressurization. The weight and volume penalty to be paid, however, was not so obvious, and a program to investigate this problem was being pursued at the same time as experimentation with various dielectrics was being performed. The TX filter was finally sealed at one atmosphere with a 90 percent nitrogen, 10 percent helium gas mixture. Subsequently, a leak rate of $\approx 1 \times 10^{-8}$ cc/sec of helium was measured at one atmosphere differential while the filter was in a vacuum chamber. Assuming a constant leak rate, this assures us that the filter will be maintained at near atmospheric pressure for at least 10-year operation, which is twice the 5-year design goal. The mechanical design of the sealed filter will be discussed in a later section.

One of the problems associated with pressurizing the filter was the probability that the gas-filled sealed filter when placed in a vacuum would undergo tuning changes due to deflections of the filter covers and walls. Since it was necessary to use the same filter for both vacuum and atmospheric testing and operation, it was determined experimentally that an allowed cover

deflection of 0.1 inch would still permit the filter to be used in both situations. The completed filter design had a measured cover deflection of only 0.060 inch at one atmosphere differential, thus ensuring minimal detuning. The TX filter was tuned while at one atmosphere differential pressure, and the measured change in tuning was negligible when the filter was used at zero pressure differential.

Since the BEC filter was to operate at a power level of approximately 10 watts, the multipactor problem was not so severe as in the TX case. The regions susceptible to multipactor at this power level are in the capacitance gaps at the ends of the resonant elements. Tests indicated that the filter operation was normal at the design power level of 10 watts; however, at lower levels of 2 to 5 watts, multipactor did occur.

The solution to this problem was to employ a slightly shorter resonant rod in the filter, which increased the capacitance needed for resonance. In this way, the capacitor gap dimension was made small enough to effectively suppress the multipactor in vacuum without causing ordinary breakdown at rated power in air.

Figure 3 shows plots of the measured response of the filters in the triplexer configuration. The flight REC, BEC, and TX filters exhibit approximately 0.5-dB insertion loss in their respective pass bands and BEC/TX mutual rejections of approximately 40 dB. The TX filter also rejects the TLM frequency by 40 dB. The difference between the BEC and TX pass-band losses is caused by the longer coaxial line between the BEC filter and the junction box.

Figure 4 shows the TX filter box before the cover was welded in place. Figure 5 is a photograph of the cover showing the stiffening members which will be described in detail later.

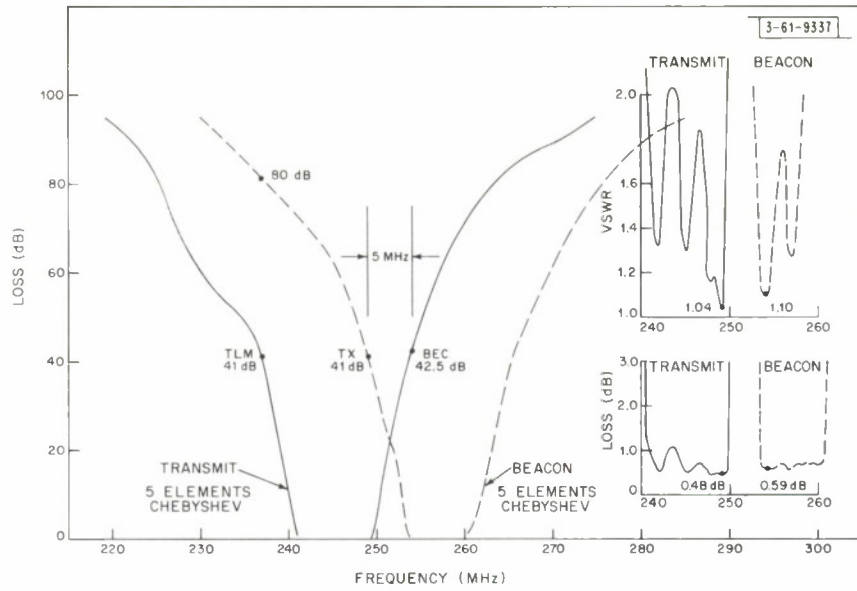
Both filters are constructed of aluminum, copper-plated for reduced RF loss and then gold-flashed to inhibit corrosion. Both BEC and TX filters are approximately $18 \times 12 \times 2\frac{1}{2}$ inches. The flight pressurized TX filter weighs 10.2 pounds, and the unpressurized BEC filter weighs 7.6 pounds. Figure 6 shows the internal configuration of the BEC filter. The shortened resonator rod and capacitor gap are clearly shown here.

II. RECEIVE FILTER

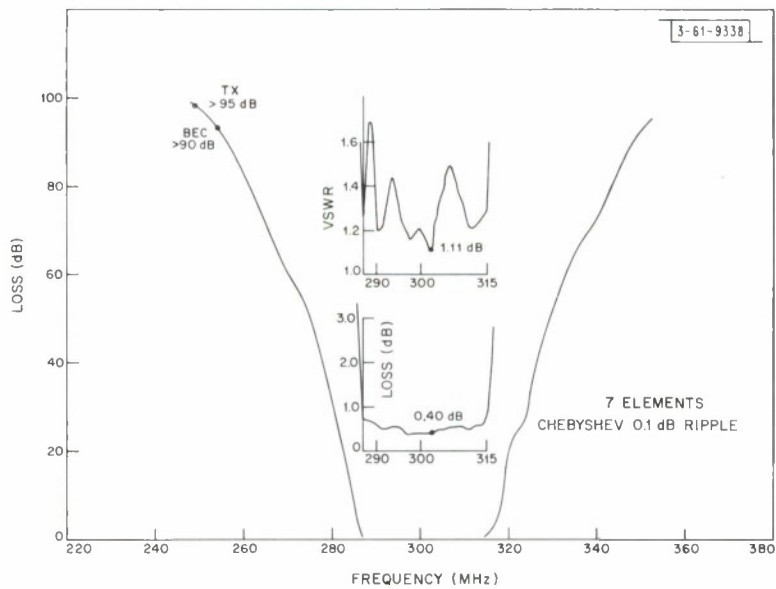
The design technique for the REC filter is identical to that used for the LES-5 receive filter. Several calculations of Chebyshev and equal-element configurations showed that the optimum filter design was a 7-element Chebyshev type with a ripple factor of 0.1 dB. The REC frequency is placed at about the center of the 25-MHz pass band. As seen in Fig. 3(b), the triplexer pass-band loss of the REC filter is approximately 0.5 dB throughout the 25-MHz bandwidth. The measured loss at the REC frequency is 0.4 dB with an input VSWR of 1.11. Construction was similar to the TX, BEC filter except for the over-all size. The REC filter is about 11 inches square by $1\frac{1}{4}$ inches deep and weighs approximately $3\frac{1}{4}$ pounds. Figures 7 and 8 show the details of the REC filter.

III. TRIPLEXER

The triplexer junction is a copper-plated, gold-flashed aluminum box into which four "OSM" panel jack connectors are mounted and then soldered together. By adjusting line lengths L_1 , L_2 , and L_3 (see Fig. 1), the input impedances of each filter at the critical frequencies were transformed to open circuits at the common junction. Line lengths L_1 , L_2 , and L_3 were experimentally adjusted to give the best over-all performance at TX, BEC, and REC frequencies.



(a)



(b)

Fig. 3. Measured response of (a) transmit and beacon interdigital filters; (b) receive interdigital filter.

Fig. 4. LES-6 TX filter.

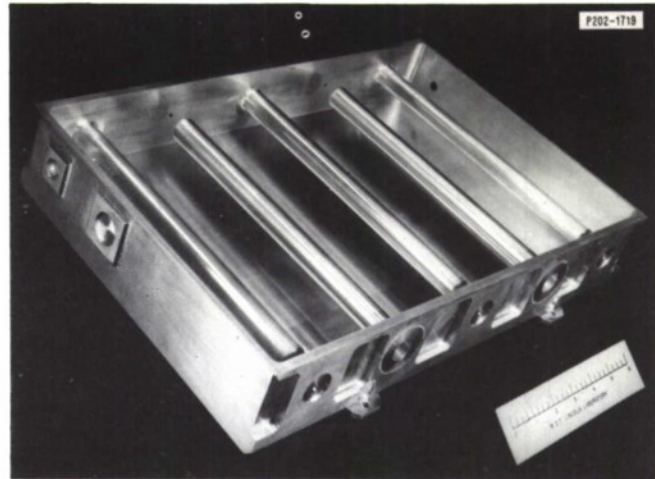


Fig. 5. LES-6 TX filter cover.

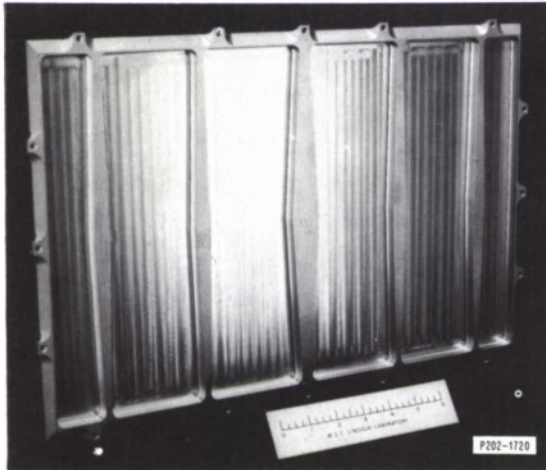
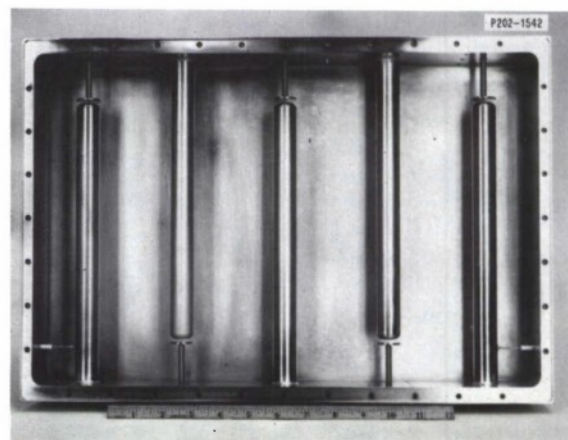


Fig. 6. LES-6 beacon bandpass filter.



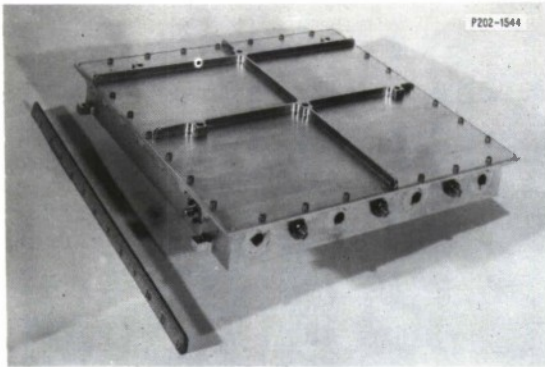


Fig. 7. LES-6 receive bandpass filter.

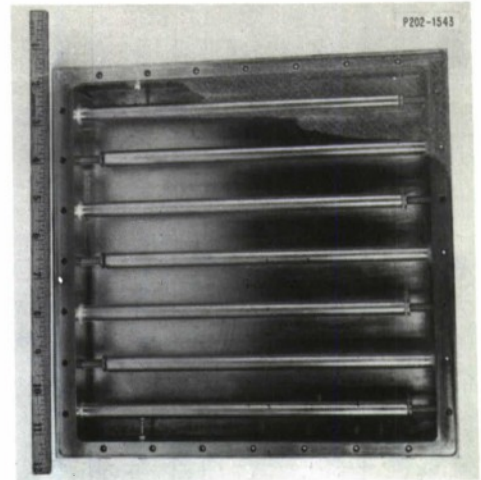


Fig. 8. LES-6 receive bandpass filter with cover removed.

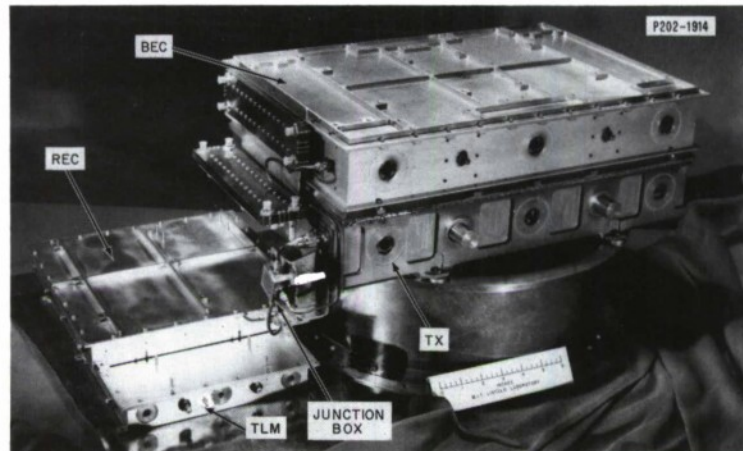


Fig. 9. Completed triplexer assembly.

Figure 9 is a photograph of a completed flight-qualified triplexer assembly on a partial mockup of the satellite platform. Two completely assembled triplexers were successfully flight-qualified by being subjected to thermal cycling, acceptance vibration, and high-power testing in air and vacuum.

IV. MECHANICAL DESIGN

The basic physical configuration of the TX filter ($18 \times 3\frac{1}{2} \times 12$ inches) did not lend itself to optimum pressure vessel design. However, the limitations of schedule, satellite configuration, and electrical design prevented any major deviations from its original design. Preliminary analysis indicated that a major effort would be required in the design of the two large flat surfaces of the filter.

In order to establish design constraints, it was necessary to determine the allowable cover deflection (large flat surface), the cover thickness, and the final operating pressure. Tests were conducted on a prototype filter to determine the maximum amount of deflection that could occur without seriously affecting the filter's electrical characteristics. The midpoint of the prototype cover was subjected to several outwardly directed point loads, and the filter was tested electrically at each of these loads. Although the deflection pattern on the flight unit would differ slightly as a result of a uniformly distributed load, the maximum acceptable midpoint deflection was determined to be 0.1 inch. The maximum cover thickness of 0.5 inch was determined by dimensional limitations within the satellite. A space of $\frac{1}{8}$ inch was provided on the top and bottom of the filter to allow for the surface deflections.

The design goal for operating pressure was set at one atmosphere to allow for a large breakdown safety margin and because of the convenience of testing the filter with this pressure. With an internal volume of approximately 8 liters, an atmosphere of 90 percent nitrogen, 10 percent helium, and a minimum leakage rate of 1×10^{-6} cc/sec of helium, the filter would have a lifetime of the order of 100 years.

A cover pattern consisting of 13 ribs, 0.5 inch wide, was assumed for the first analysis. Because of symmetry, it was necessary to study only a quarter section. It was further assumed that the cover was composed of discrete beams cantilevered at one end with a redundant support and bending moment as shown in Fig. 10. The redundant pin joint support was required to simulate the axial load capacity of the vertical wall, and the additional cantilever beam length was required to simulate the wall bending stiffness. Each beam was divided into an arbitrary number of lengths (7 equal lengths in this case) such that the bending moments, shear loads, and deflections could be studied at various points in the beam. The model was then analyzed on an IBM 360 computer using Jet

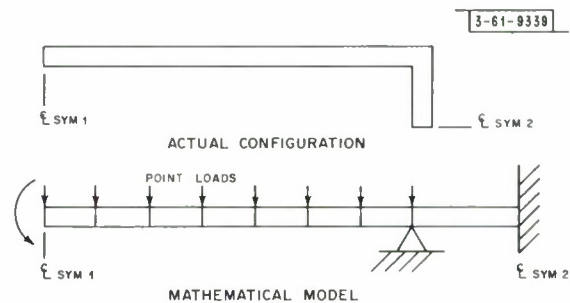


Fig. 10. Point load beam analysis model.

Propulsion Laboratory's stiffness Matrix Structural Analysis computer program. This program requires the following as input data:

- (1) Coordinates of the joints,
- (2) Geometric and elastic properties of the members,
- (3) Location of the restraints,
- (4) Inertias at the joints,
- (5) Static loads at the joints,
- (6) Acceleration of a joint during free vibration in a normal mode.

The output from this program is as follows:

- (1) Deflections and member stresses for static loadings,
- (2) Frequencies, mode shapes, and member stresses during free vibration in normal modes.

The results of the initial computer runs indicated that the welded junction of the cover plate and the vertical wall on the beam which was in the center of the cover had a large bending moment.

To determine the effect of this moment on the weld, samples as shown in Fig. 11 were loaded in an Instron testing machine. The data taken from these tests indicated that the bending moment as determined in the analysis would cause a fracture of the weld. In order to reduce the bending moment of the weld, the beams were then tapered.

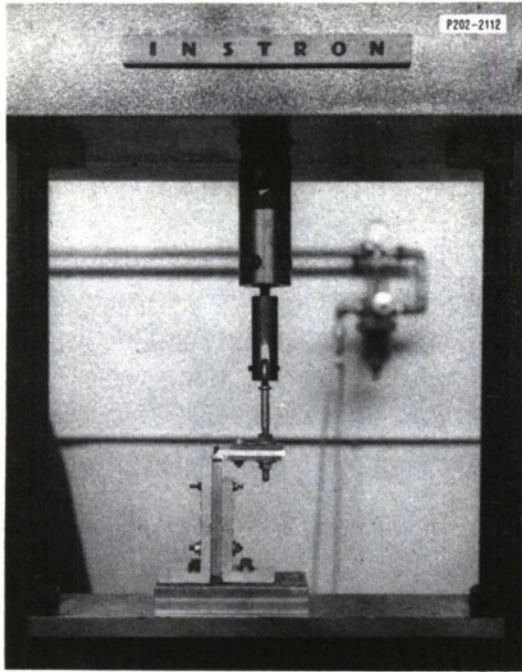


Fig. 11. Test configuration to determine EB weld allowables.

At this point, it was found that the computer "turn around" time would prohibit an optimum tapered beam design in the time allotted. It was therefore decided to derive an expression for the weld bending moment as a function of a uniform pressure load on a tapered beam, which had the same restraints as the mathematical model, and to implement this expression on the Time Sharing Computer. The Appendix presents the derivation of the redundants which were then programmed on the computer to result in the weld bending moment for various beam tapers.

This technique resulted in the final design. The deflection of the center of the plate as determined by this analysis was found to be 0.055 inch as compared with a measured value of 0.060 inch.

V. FABRICATION

Electron Beam (EB) welding was chosen as the method for hermetically sealing the filter because of its advantages, in this case, over other methods. In comparison with O-ring seals, welding allows for simpler joint design, less difficult leak-detection techniques, less susceptibility to damage because of surface imperfections, and longer-term reliability. The advantages of EB welding over other welding methods are low-energy input (important in preventing damage to glass-to-metal sealed connectors), relatively little distortion, large depth-to-width penetration ratio, and the fact that the welding is performed in a vacuum clean environment.

The filter was fabricated from 2024-T351 aluminum alloy because of its light weight, good strength, and ability to be EB welded without the use of filler material. As mentioned previously, samples of all the welded joints were tested to obtain information on the welding energy,

resultant distortions, and the strength of the joints. The minimum tensile strength at failure was 41,500 psi, thereby providing a safety factor of two over the design maximum of 20,000 psi.

The most critical component in the filter was the glass-to-metal hermetically sealed RF coaxial connector. Fortunately, a type TNC connector which was suitable electrically and which had been specifically designed for EB welding to aluminum was commercially available. However, on samples that were welded and from the experience of prior users of this connector, it was found that the glass-to-metal interface in the connectors could be thermally damaged in the EB welding process. To prevent this failure from occurring on the flight filter, the connectors were first welded to a washer-shaped flange. This served to increase the heat transfer path from the glass-to-metal seal to the final weld performed on the connector. No connector failures occurred on the completed filter assemblies using this procedure.

However, difficulties were encountered during the welding of the filter cover. Previously welded samples of this joint were excellent, but the additional weight of the filter and fixturing revealed a fault in the positioning table. The result of this was a slower welding speed and, therefore, excessive penetration of the weld. The cover of this filter had to be machined off and replaced.

The first series of leak tests was qualitative in nature. It consisted of pressurizing the filter (4 to 5 psig) with helium and probing the outside with a vacuum line attached to the leak detector. The fast response time of this technique resulted in the accurate location of leaks. Initially, the filters were leak-tested at each stage of assembly; however, this required that unwelded joints be temporarily sealed which, in many cases, caused contamination of the joints and subsequent difficulties in welding. Since all the joints were readily accessible for repair, the filter was completely welded before any leak tests were performed. Final absolute leak-rate measurements were obtained by sealing the unit and placing it in a vacuum system attached to a calibrated helium leak detector. The measured leakage rate for the flight unit was 1×10^{-8} cc/sec of helium.

In the first series of random vibration tests, the resonant elements failed at their cantilever supports. Dielectric supports at the free end were undesirable because of their perturbing effect on the electrical characteristics, thus requiring retuning and/or redesign of the filter. By experimentation it was found that a substantial reduction in the amplitude of the element vibration was effected by placing loose-fitting rubber tubing inside the element. The tubing is outside the filter electrically and has no effect on the RF performance. The size, durometer, and wall thickness were not critical parameters. The action of the rubber tubing appeared to be similar to that of a damper and dynamic vibration absorber and, in our case, successfully prevented element failure due to vibration.

ACKNOWLEDGMENT

The authors wish to thank B. F. LaPage and R. W. Purdy for their technical assistance.

REFERENCES

1. S. B. Cohn, "Direct-Coupled-Resonator Filters," Proc. IRE 2, 187 (1957).
2. A. Sotiropoulos, "LES-5 Triplexer," Technical Report 438, Lincoln Laboratory, M. I. T. (31 August 1967), DDC 823174.
3. "The Study of Multipactor Breakdown in Space Electronic Systems," Hughes Aircraft Company, NASA, CR-448 (July 1966); CR-71999, Vol. II (April 1965).

APPENDIX

The beam shown in Fig. 12 is an approximation of a tapered-beam section of the filter. The tapered section of the mathematical model is divided into n (12 in this case) beams of length ℓ .

The bending moment for beams 1 through 12 is

$$M_x = R_1 + \frac{(n-1)^2 P \ell^2}{2} + (n-1) P \ell x + \frac{P x^2}{2} \quad .$$

The bending moment in beam 13 (Fig. 13) is

$$M_{13} = R_1 + 144 \frac{P \ell^2}{2} + (V - R_2) x + \frac{P x^2}{2} \quad ,$$

where

$$V = P (12\ell),$$

$$q = V - R_2 = 12P\ell - R_2 \quad .$$

The total bending energy is given by

$$U_t = \sum \frac{M^2 ds}{2EI} \quad .$$

Substituting the moment equations results in the following:

$$U_t = \int_0^\ell \sum_{n=1}^{12} \left\{ \left[R_1 + \frac{(n-1)^2 P \ell^2}{2} + (n-1) P \ell x + \frac{P x^2}{2} \right]^2 \frac{dx}{2EI_n} \right\} \\ + \int_0^{\ell_{13}} \left[R_1 + \frac{144 P \ell^2}{2} + (V - R_2) x + \frac{P x^2}{2} \right]^2 \frac{dx}{2EI_{13}}$$

Equating the partial differential of the energy with respect to each redundant to zero results in two simultaneous equations which can be solved for R_1 and R_2 :

$$\frac{\partial U_t}{\partial R_2} = \int_0^{\ell_{13}} \left[R_1 + \frac{144 P \ell^2}{2} + (V - R_2) x + \frac{P x^2}{2} \right] (-x) \frac{dx}{EI_{13}} \\ = \int_0^{\ell_{13}} \left[R_1 x + 72 P \ell^2 x + 12 P \ell x^2 - R_2 x^2 + \frac{P x^3}{2} \right] dx = 0 \quad .$$

Integrating,

$$\frac{R_1 \ell_{13}^2}{2} + \frac{72 P \ell^2 \ell_{13}^2}{2} + \frac{12 P \ell \ell_{13}^3}{3} - \frac{R_2 \ell_{13}^3}{3} + \frac{P \ell_{13}^4}{8} = 0 \quad ,$$

$$R_2 = \frac{3R_1}{2\ell_{13}} + \frac{108 P \ell^2}{\ell_{13}} + 12 P \ell + \frac{3 P \ell_{13}}{8} \quad ,$$

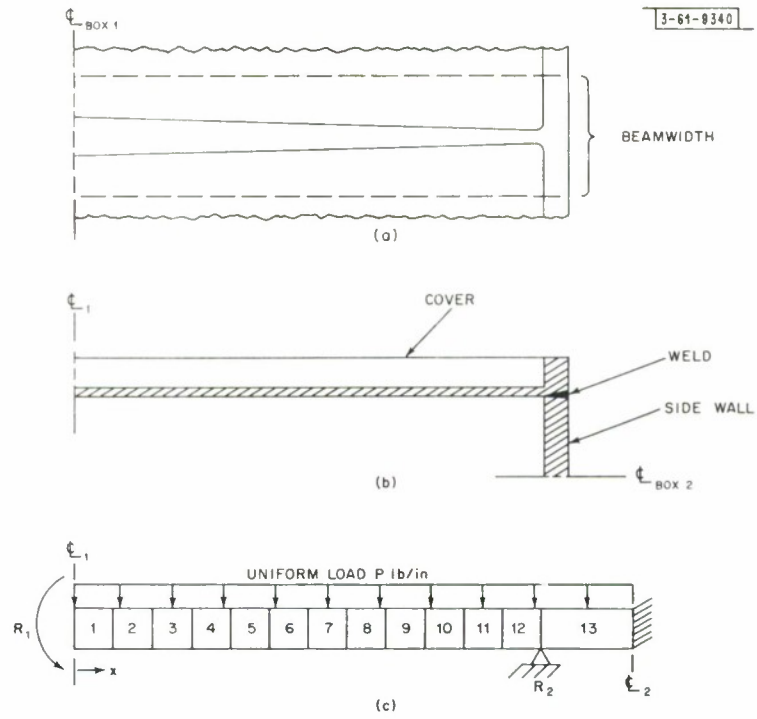


Fig. 12. Uniform load tapered beam analysis model: (a) actual, top view; (b) actual, side view; (c) mathematical model, side view.

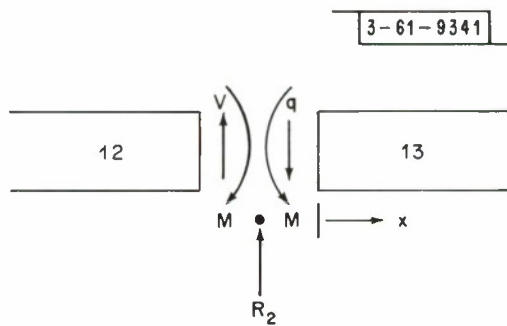


Fig. 13. Welded joint free body diagram.

$$\frac{\partial U_t}{\partial R_1} = 0 = \int_0^\ell \sum_{n=1}^{12} \left\{ \left[R_1 + \frac{(n-1)^2 P \ell^2}{2} + (n-1) P \ell x + \frac{P x^2}{2} \right] \frac{dx}{EI_n} \right\} \\ + \int_0^{\ell_{13}} \left[R_1 + \frac{144 P \ell^2}{2} + 12 P \ell x - R_2 x + \frac{P x^2}{2} \right] \frac{dx}{EI_{13}}$$

Substituting R_2 and integrating,

$$\sum_{n=1}^{12} \left\{ \left[R_1 \ell + \frac{(n-1)^2 P \ell^3}{2} + \frac{(n-1) P \ell^3}{2} + \frac{P \ell^3}{6} \right] \frac{1}{I_n} \right\} \\ + \left[R_1 \ell_{13} + 72 P \ell^2 \ell_{13} + 6 P \ell \ell_{13}^2 - \frac{3 R_1 \ell_{13}}{4} - 54 P \ell^2 \ell_{13} \right. \\ \left. - 6 P \ell \ell_{13}^2 - \frac{3 P \ell_{13}^3}{16} + \frac{P \ell_{13}^3}{6} \right] \frac{1}{I_{13}}$$

$$R_1 \ell \sum_{n=1}^{12} \left(\frac{1}{I_n} \right) + \sum_{n=1}^{12} \left\{ \left[(n-1)^2 \frac{P \ell^3}{2} + (n-1) \frac{P \ell^3}{2} + \frac{P \ell^3}{6} \right] \frac{1}{I_n} \right\} \\ + \frac{R_1 \ell_{13}}{4 I_{13}} + \frac{18 P \ell^2 \ell_{13}}{I_{13}} - \frac{P \ell_{13}^3}{48 I_{13}} = 0$$

$$R_1 = \frac{- \left[\frac{18 P \ell^2 \ell_{13}}{I_{13}} - \frac{P \ell_{13}^2}{48 I_{13}} \right] - \sum_{n=1}^{12} \left[(n-1)^2 \frac{P \ell^3}{2} + (n-1) \frac{P \ell^3}{2} + \frac{P \ell^3}{6} \right] \frac{1}{I_n}}{\left[\ell \sum_{n=1}^{12} \left(\frac{1}{I_n} \right) + \frac{\ell_{13}}{4 I_{13}} \right]}$$

Substituting the resulting expressions for R_1 and R_2 into the moment equations and solving them results in the bending moment distribution for the tapered beam. Due to the fact that a summation is required to solve R_1 and R_2 , and in order to optimize the beam's taper, the expressions were programmed on the CMS time-sharing computer. By an iterative process of changing the beam taper and analyzing the resultant bending moment distribution, a final taper beam design was chosen that satisfied the strength requirements of the welded joint.

